A global summary of seafloor topography influenced by internal-wave induced turbulent water mixing

by Hans van Haren and Henk de Haas

NIOZ Royal Netherlands Institute for Sea Research, P.O. Box 59, 1790 AB Den Burg, the Netherlands.
e-mail corresponding author: hans.van.haren@nioz.nl

Short summary. Turbulent water motions are important for the exchange of momentum, heat, nutrients, and suspended matter in the deep-sea. The shape of marine topography influences most water turbulence via breaking internal waves at 'critically' sloping seafloors. In this paper, the concept of critical slopes is revisited from a global internal wave-turbulence viewpoint using seafloor topography- and moored temperature sensor data. Potential robustness of the seafloor-internal wave interaction is discussed.

Abstract. Turbulent water motions are important for the exchange of momentum, heat, nutrients, and suspended matter including sediments in the deep-sea that is generally stably stratified in density. To maintain ocean-density stratification, an irreversible diapycnal turbulent transport is needed. The geological shape and texture of marine topography is important for water mixing as most of deep-sea turbulence is generated via breaking internal waves at sloping seafloors. For example, slopes of semidiurnal internal tidal characteristics can 'critically' match the mean seafloor slope. In this paper, the concept of critical slopes is revisited from a global internal wave-turbulence viewpoint using seafloor topography- and moored high-resolution temperature sensor data. Observations suggest that turbulence generation via internal wave breaking at 5±1.5% of all seafloors is sufficient to maintain ocean-density stratification. However most, >90%, turbulence contribution is found at supercritical, rather than the more limited critical, slopes measured at 1′-scales that cover about 50% of seafloors at water depths < 2000 m. Internal tides (~60%) dominate over near-inertial waves (~40%), which is confirmed from comparison of NE-Atlantic data with East-Mediterranean data (weak tides). Seafloor-elevation spectra show a wavenumber (k) fall-off rate of k^{-3}, which is steeper than previously found. The fall-off rate is even steeper, resulting in less elevation-variance, in a one-order-of-magnitude bandwidth around k_T=0.5 cycle-per-km. The corresponding length is equivalent to the internal wave excursion length. The reduction in seafloor-elevation variance seems associated with seafloor-erosion by internal wave breaking. Potential robustness of the seafloor and internal wave interaction is discussed.

1 Introduction

The present ocean exists for millions of years, and so seemingly do its seafloor shape and its water flows including properties like the stable vertical stratification in density from the heating by the sun. Because sedimentation and erosion of suspended matter in the ocean are subject to water flows that partially depend on interaction with the seafloor, one may question the stability or variability of seafloor-shape and water flow properties. Compared with geological time scales of variation (sedimentary: years; rocks: centuries/millennia), water flows in the deep ocean are fast fluctuating (meso-scale eddies: weeks/months; tides: hours/days). However, that does not preclude potential interactions between water flows and topographic bed-forms, with local results such as sand ripples and sediment waves (e.g., Trincardi and Normark, 1988; Puig et al., 2007).

As seafloor-erosion by resuspension is mainly driven by intense water turbulence, and seafloor-deposition by weak turbulence, seafloor-shaping such as contourite morphology (e.g., Rebesco et al. 2014; Chen et al., 2022) depends on dominant ocean-turbulence generation processes. Following, e.g., Wunsch (1970), Eriksen (1982), Thorpe (1987), Klymak and Moum (2003), Hosegood et al. (2004) and Sarkar and Scotti (2017), ocean turbulence above sloping seafloors is predominantly generated via the breaking of internal water waves. The turbulence produced by the breaking of internal waves is considered vital for the global ocean meridional overturning circulation (e.g., St. Laurent et al., 2012). Such waves are mainly supported by the stable vertical density stratification. Their effects on shaping ocean's seafloor morphology cannot be overestimated (Rebesco et al., 2014).

More in general, balancing feed-back interaction leading to a quasi-stable equilibrium is expected between the slopes of seafloor topography and long-lasting ubiquitous water-flows, e.g., generated by internal waves that are notably driven by oscillating tides and the waves' density-stratification support. In their pioneering works, Bell (1975a,b) from an internal wave generation perspective, Cacchione and Wunsch (1974) and Eriksen (1982; 1985) from an internal wave breaking perspective, and Cacchione and Southard (1974) from a geological

94 formation perspective, suggested that a ‘critical’ match exists between the mean angles of
95 deep-sea topography slopes and those of internal wave ‘characteristics’.

96 Because internal water waves are essentially three-dimensional (3D) phenomena, which
97 distinguishes them from 2D surface waves, their energy propagates along characteristics, i.e.
98 paths that slope to the horizontal as a function of wave frequency and stratification. Internal
99 waves can reflect off a seafloor slope, but due to angle-preservation with respect to gravity
100 instead of bottom-normal internal wave energy is thought to build-up when the two slopes are
101 identical, yielding potential propagation parallel to a critical seafloor slope (Cacchione and
102 Wunsch, 1974). When the seafloor slope is larger than the internal wave slope it is
103 supercritical, when it is smaller than the internal wave slope it is subcritical (for that particular
104 wave frequency under given stratification conditions).

105 While Bell (1975a,b) considered seafloor elevation statistics on internal wave generation,
106 the works by Cacchione and co-authors considered seafloor shaping by internal wave
107 motions. It was found that the average seafloor slope amounts 3±1°, which matches the
108 characteristics slope of energy propagation direction of internal waves at semidiurnal tidal
109 frequency for stratification from around 1700 m below the sea surface, which is about half the
110 average water depth.

111 While the above finding is remarkable and has led to numerous investigations on critical
112 reflection of internal waves, it is challenged from various perspectives. This is because: First,
113 exactly matching ‘critical’ slopes for dominant internal tides are few and far between and
114 cannot persist in space and time because the ocean stratification varies in space and time.
115 Second, internal waves mostly break above sloping topography, very little in the ocean
116 interior (Polzin et al., 1997). Third, most ocean seafloors, i.e. 75% by area and 90% by
117 volume (Costello et al., 2010; Costello et al., 2015), occur between 3000 and 6000 m water
118 depth where density stratification is weak. Fourth, about 40% of total internal wave energy is
119 estimated at near-inertial frequencies (e.g., Wunsch and Ferrari, 2004).

120 Near-inertial waves are generated as transients following geostrophic adjustment on the
121 rotating Earth, e.g., after passing atmospheric disturbances or frontal collapses (LeBlond and

Mysak, 1978). Their occurrence shows a strong variability with location, e.g., demonstrating large near-surface generation in western boundary flows and much weaker generation in eastern ocean-basins (Watanabe and Hibiya, 2002; Alford, 2003). As near-inertial waves have a quasi-horizontal component, virtually all seafloor slopes are steeper: They are supercritical (for near-inertial waves). These observations demand further investigation in the seafloor/internal wave-turbulence interaction, also considering the potential impact on climate variability and the contribution of oceans in distributing heat therein.

Detailed ocean observations indicate that most intense turbulence and sediment resuspension over sloping seafloors is not generated by frictional (shear-)flows (as suggested by, e.g., Cacchione et al., 2002), but by nonlinearly deformed internal waves breaking (e.g., Klymak and Moum, 2003; Hosegood et al., 2004). Such nonlinear internal wave breaking predominantly generates buoyancy-driven convection-turbulence. Growing evidence suggests that most breaking occurs at slopes that are just supercritical (van Haren et al., 2015; Winters, 2015; Sarkar and Scotti, 2017).

Any interaction between seafloor shape and texture and water-flow turbulence is expected to vary on geological time scales, because besides deep-sea topography also ocean-interior vertical density stratification exists as long as the oceans do: The ocean is not and has not been a pool of stagnant cold water underneath a thin layer of circulating warm water heated by the sun (Munk and Wunsch, 1998). The question is how stable a balance of such an interaction can be, e.g., between internal waves that are supported by varying stratification and seafloor topography. Is the balance an optimum, or rather a marginal equilibrium, like the marginally stable stratification supporting maximum destabilizing internal shear in shelf seas (van Haren et al., 1999)? Especially given relatively rapid changes, such as Earth-surface heating attributed to mankind, does a balance buffer any modifications: to topography (long time scale), vertical density stratification (medium time scale), and/or to water-flow (short time scale)? Prior to being able to (mathematically) predict any potential tipping point of a balance, the physical processes need to be understood that contribute to a balance. Amongst

149 other deep-sea processes, this involves the physics of internal wave-formation and -breaking
150 into turbulence generation upon interaction with topography and restratification of density.

151 In this paper, we discuss the (im)possibility of relating seafloor statistics with open-ocean
152 density stratification and internal wave breaking as observed in recent measurements. We
153 revisit concepts of deformation, erosion, and sedimentation, of deep seafloor topography in
154 interaction with internal waves, with vertical density stratification, with turbulence, with
155 ocean's heating/cooling, and consider the (in)stability of these interactions. Instead of Bell's
156 (1975a,b) perspective of internal wave generation, above NE-Pacific abyssal hills, we adopt
157 the perspective of internal wave breaking and turbulence generation through moored high-
158 resolution temperature observations above a wide variety of deep-ocean topography. We also
159 adopt a geological seafloor topography perspective using some detailed multibeam
160 echosounder and global seafloor elevation repository data. An attempt is made to consider the
161 statistical spread of different variables.

162

163 *1.1 Some considerations on ocean variability and internal wave-topography interactions*

164 A large variability over two orders of magnitude exists in stable ocean-density
165 stratification ($\sim N^2$), albeit a gradual, not constant, decrease with increasing depth is observed
166 in buoyancy frequency N, a measure of stability of a fluid to vertical displacements (e.g.,
167 Wüst, 1935; Wunsch, 2015). This gradual decrease with depth results in a corresponding
168 increase in the slope β to the horizontal of characteristics along which internal wave energy
169 propagates. For general ocean stratification this slope is approximately inversely proportional
170 to N (e.g., LeBlond and Mysak, 1978),

171 $$\beta = \sin^{-1}((\omega^2-f^2)^{1/2}/(N^2-f^2)^{1/2}), \quad (1)$$

172 for freely propagating linear internal waves at frequency ω. Here, f denotes the inertial
173 frequency or Coriolis parameter, the vertical component of planetary vorticity. Internal waves
174 and sub-inertial water-flows deform the stratification locally, thereby making N a function of

time and space N = N(x,y,z,t). The consequences of variability for β will be explored from observations in Section 3.

Several global internal wave statistics can be given. The rms-mean deep-sea topography slopes of 3±1° (Bell, 1975b; Cacchione et al., 2002) roughly match the mean slope of (linear) semidiurnal internal tide characteristics, provided the latter are computed using in (1) a value of $N \approx 2\times10^{-3}$ s^{-1} for mid-latitude locations. Such N is found approximately around z = -1700 m in the open ocean, which has a mean depth of H = 3900 m outside shelf seas (Wunsch, 2015). In these open-ocean mid-depth waters internal wave breaking and thus turbulence generation are sparse (e.g., Gregg, 1989; Polzin et al., 1997; Kunze, 2017).

Observational evidence suggests that vigorous turbulent mixing by internal wave breaking is only found in a limited height of h = 100-200 m (e.g., Polzin et al., 1997) above the seafloor, coarsely estimated to occur over only 5-15% of all seafloor slopes to maintain the ocean stratification (e.g., van Haren et al., 2015). As for relevant length scales: Although satellite altimetry observations demonstrate low-mode internal tides having wavelengths O(100) km (e.g., Dushaw, 2002; Ray and Zaron, 2016), the excursion length of internal tides is typically O(1) km and which may prove important for turbulence generation and thus sediment erosion of seafloor-texture and -topography.

Especially the smaller length scale O(1) km may fit the spectral analysis of NE-Pacific seafloor elevation, which is found to fall-off with horizontal wavenumber (k) like $k^{-2.5}$ (Bell, 1975a), later corrected to k^{-2} (Bell, 1975b). The latter is interpreted as a random distribution of hills in which the energy of formation is distributed uniformly over all sizes. Internal wave generation is found by Bell (1975a,b) mainly between $0.33 < k < 3$ cpkm (short for cycles per kilometer). Here, we add that this roughly matches a band with increased spread of topographic-height variance between $0.15 < k < 1$ cpkm, which is visible in the presented data albeit not mentioned by Bell (1975a,b).

Geomorphology influences water-flow and turbulence and these in turn influence sediment erosion and deposition and thus (fine-tuning) the geomorphology. So, if enough

time is available (after all, geologists think in terms of millions of years), one will eventually reach an equilibrium. The major geomorphological processes occur on a much larger timescale than the adaptation of water-flows, and any ocean will "always" be in an equilibrium situation because the flows adapt relatively quickly to a slow geological change.

Thus, following variations in ocean internal wave turbulence, seafloor topography will adapt. However, the ocean also interacts with a faster adaptive/varying system: the atmosphere. Temperature changes in water are slower than in air because of the larger heat capacity of the former. Nevertheless, a direct correspondence with changes in vertical density (temperature) stratification is not evident as larger stratification can support more internal waves and thus potentially more turbulent wave breaking that may restore a balance. (It is noted that atmosphere dynamics is not driven by the ocean, except indirectly by modification of moisture content).

The dominant source of ocean internal waves are tides (e.g., Wunsch and Ferrari, 2004). The local seafloor slope γ, computed over a certain horizontal distance, is supercritical for linear freely propagating semidiurnal lunar M_2 internal tidal waves, when $\gamma > \beta_{M2}$, using $\omega_{M2} = 1.405\times10^{-4}\ s^{-1}$ in (1).

A secondary source are near-inertial waves $\omega \approx f$, which generally have a near-horizontal slope of characteristics. Only in very weak stratification N = O(f), some near-inertial slopes may become large enough to distinguish various subcritical slopes for such waves. However, under weakly stratified conditions, terms involving the horizontal Coriolis parameter are no longer negligible, and two distinctly differently sloping characteristics $\mu_\pm$ of internal wave energy propagation result (e.g., LeBlond and Mysak, 1978; Gerkema et al., 2008):

$$\mu_\pm = (B \pm (B^2\text{-}AC)^{1/2})/A, \qquad (2)$$

in which $A = N^2 - \omega^2 + f_s^2$, $B = ff_s$, $C = f^2 - \omega^2$ and $f_s = f_h \sin\alpha$, α the angle to latitude (φ). The slopes of $\mu_\pm$ indicate directions to the horizontal in a more general way than the single slope (1) obtained under the traditional approximation.

For large $N >> f$, the slope of the two characteristics in (2) approach each other and their slope approaches β in (1). Under conditions $N < 10f$ and latitudinal propagation ($\alpha = \pi/2$), one of the characteristics in (2) becomes quasi-horizontal for which virtually all seafloor slopes are supercritical, and the other becomes more steeply sloping.

The impact of (2) may also not be ignorable for semidiurnal tides in weakly stratified waters around mid-latitudes. With the full non-approximated equations (2) and a stratification of about $N = 8f$, which is typical in waters near the 3900-m mean depth of the ocean seafloor, the slope (1) of $\beta_{M2} = 9.1°$ rather becomes 10.3° and 7.9° for up- and down-going characteristics $\mu_{\pm}$, respectively (for $|\varphi| = 37°$).

This spread of about ±13% is a substantial addition to variation in seafloor slope-criticality and becomes larger at weaker stratification ($N < 8f$) and smaller at stronger stratification ($N > 8f$). Although the vertical density stratification is generally a monotonic decreasing function with increasing depth, deviations occur, such as in some, e.g. equatorial, areas around 4000 m where larger N is found than above and below, and which is attributed to the transition between deep Arctic waters overlying most dense Antarctic waters (King et al., 2012).

The ubiquitous linear internal waves at various frequencies $f \leq \omega \leq N$ (for $N > f$) provide ample options for wave-wave and wave-topography interactions. While some interactions seem too slow, the wave-topography interactions above sufficiently steep topography show strongly nonlinear wave deformation resulting in convection-turbulence when the ratio of particle velocity (u) over phase speed (c) amounts $u/c > 1$: A fast process. Propagation of such highly nonlinear internal waves is beyond the scope here, but the turbulence dissipation rate of internal wave energy affecting seafloor sediment is not.

Although the ocean and deep-seas are overall turbulent in terms of large bulk Reynolds numbers Re well exceeding $Re > 10^4$ and more generally $Re = O(10^6)$, it is a challenge to study the dominant turbulence processes. As the ocean is mainly stably stratified in density, which hampers the vertical size-evolution of fully developed three-dimensional isotropic

turbulence, it is expected that in the deep-sea and in strained thick layers stratification is much weaker resulting in near-neutral conditions of (almost) homogeneous waters in which $N \approx f$. Under such conditions turbulent overturns may be slow and large and may govern more the convection-turbulence process, rather than the shear-turbulence process that dominates under well-stratified conditions $N >> f$ across thin layers in the interior and in frictional flows over the seafloor.

1.2 Internal wave energy dissipation perspective

According to Wunsch and Ferrari (2004), in follow-up from Munk and Wunsch (1998), the currently best estimate for global internal wave power to be dissipated is 0.8 TW (1 TW $=10^{12}$ W) for internal tides and about 0.5 TW for wind-enforced mainly near-inertial waves. These numbers are determined to within an error of a factor of 2, although this error range is probably smaller for internal tides (since the rather precise determination of energy loss of the Moon-Earth system).

If we distribute this amount of power over the entire global ocean with a surface of 3.6×10^{14} m^2 (e.g., Wunsch, 2015), the vertically integrated dissipation rate amounts for internal tides,

$$2.2\times10^{-3} \text{ W m}^{-2} = \int \rho\varepsilon \, dz, \quad (3)$$

and 67% of that value for inertial waves. In (3), $\rho = 1026$ kg m^{-3} denotes an average density of ocean-water and ε the kinetic energy turbulence dissipation rate.

If we suppose that (3) is distributed over the entire vertical water column, over a mean water height of $H = 3900$ m (Costello et al., 2010; Wunsch, 2015), a global mean rate to dissipate the internal tidal energy is required of,

$$\varepsilon_H = 6\times10^{-10} \text{ m}^2 \text{ s}^{-3}, \quad (4)$$

and 67% of this value for near-inertial waves. As a result, the entire global-mean turbulence dissipation rate of all internal waves (generated by internal tides and near-inertial waves) is

about 10^{-9} m^2 s^{-3}. This is equivalent to the mean value found after evaluation of 30,000 ocean profiles on internal wave turbulence (Kunze, 2017).

Given a mean mixing efficiency of $\Gamma = 0.2$ over values distributed over one order of magnitude (Osborn, 1980; Oakey 1982; Dillon, 1982), and $N = 1.5\times10^{-3}$ s^{-1} found around open-ocean z = -1900 m, one arrives at a vertical (actually, diapycnal) turbulent diffusivity of $K_z = \Gamma\varepsilon N^{-2} = 10^{-4}$ m^2 s^{-1}, for above global internal-wave-induced dissipation rate. This is the canonical K_z-value proposed by Munk (1966) and Munk and Wunsch (1998) to maintain the ocean stratification and to drive the meridional overturning circulation.

However, according to measurements using extensive shipborne water column profiling (e.g., Gregg, 1989; Kunze, 2017) and some moored high-resolution temperature sensors (van Haren, 2019) the average open-ocean dissipation rate amounts $4\pm2\times10^{-10}$ m^2 s^{-3}, which is less than half the required value to maintain the ocean stratification. Locations are thus sought where turbulent mixing is sufficiently strong to cover at least 6×10^{-10} m^2 s^{-3} for the insufficient turbulent mixing by sparse internal wave breaking in the open-ocean interior.

It has been suggested that >99% of overall internal wave induced ε is to be found for -2000 < z < -380 m (Kunze, 2017), reasoning that in this depth zone stratification, $N^2 \propto \varepsilon/K_z$, is largest. However, ε and K_z are not necessarily (un)related, and more complex correspondence has been observed between the three parameters ε, K_z and N, e.g., in Mount Josephine data (van Haren et al., 2015). Above particularly sloping seafloors, turbulence dissipation rate is found to increase with depth (e.g., Polzin et al., 1997; van Haren et al., 2015; Kunze, 2017), with consequences for the outcome of general ocean circulation models with predicted subtle effects on upwelling near the seafloor (Ferrari et al., 2016). The internal wave breaking potency above the abundant seafloor topography led Armi (1979) and Garrett (1990) to propose that one-and-a-half orders of magnitude larger turbulence than found in the ocean-interior would be needed in a layer O(100) m above all seafloors. This suggestion did not include the particulars of dependency of internal wave turbulence intensity on stratification, slopes, and wave-nonlinearity.

Internal waves, in particular internal tides, have amplitudes of several tens of meters, which in the vicinity of sloping topography may grow over 50 m, whereby they deform nonlinearly. So, if we suppose a breaking zone of h = 100 m, one needs above all seafloors local turbulence intensity of the value of ε_H augmented by a factor of H/h = 3900/100,

$$\varepsilon_h = 2.3\pm0.7\times10^{-8}\ m^2\ s^{-3}. \quad (5)$$

This value has been observed above a (semidiurnal tidal) critical slope around H = 2500 m of Mount Josephine, NE-Atlantic Ocean (van Haren et al., 2015). But, not all seafloor-slopes show the same level of internal wave breaking, and variations in turbulence dissipation rate by a factor of 100 have been observed between sub- and supercritical slopes over horizontal distances of only O(10) km.

Potential high-turbulence locations are supercritical slopes (Winters, 2015; van Haren et al., 2015; Sarkar and Scotti, 2017) and canyons (van Haren et al., 2022), where moored observations demonstrate one order of magnitude larger tidally averaged values than ε_h of,

$$\varepsilon_{ho} = 3.5\pm1\times10^{-7}\ m^2\ s^{-3}, \quad (6)$$

due to internal tidal and near-inertial wave breaking across a larger observational height of h_o = 200±50 m above seafloors around H = 1000±200 m. About 60% of turbulence dissipation rate occurs in half an hour during the passage of an upslope propagating bore with 50-m averaged peak intensities of $10^{-5}\ m^2\ s^{-3}$ (van Haren and Gostiaux, 2012).

If such turbulence intensity as in ε_{ho} occurs in 250/3900 of mean water depth it needs to occur over only 5±1.5% of all slopes to sustain 1.67 times ε_H. The percentage-value is the mean of statistical distribution accounting for errors. This ~5% is still a considerable portion of the ocean's seafloors. If just by internal tides, because virtually all seafloors are supercritical for near-inertial waves, supercritical slopes are required to comprise 3±1% of the slopes, according to ε_H. In half-shallower waters of H = 1900 m, these percentages of slopes are reached for similar turbulence intensity over h = 125 m, but these shallower water depths present only about 10% of the ocean seafloor area (Costello et al., 2010; Costello et al., 2015). We elaborate in Section 3. It is noted that we require (just) supercritical slopes for intense

turbulent internal wave breaking, not critical slopes that are limited over (much) smaller areas and are prone to vary more with space and time than supercritical slopes.

1.2.1 Variability in linear internal waves

Considering the limited occurrence of critical slopes, we address the variability in internal (tidal) wave slopes (1), $\beta = \beta(\omega, f, N, t)$. At a fixed mooring location, planetary f 'f^p' has zero variability, but relative rotational vorticity of up to $f^r = \pm 0.05 f^p$ may be introduced by (sub-)mesoscale eddy activity, so that f should be replaced by 5% variable local effective Coriolis parameter $f^{eff} = f^p + f^r$ (e.g., Kunze, 1985). Likewise, different semidiurnal tidal internal wave frequencies lead to a variation of slopes. Because solar frequency S_2 differs by 3.5% from lunar M_2, $\Delta\beta(\omega)$ varies by about 6% around mean β. (It is noted that internal M_2 cannot propagate freely very far poleward of $|\varphi| = 74.5°$ under stratified conditions using non-approximated equations: to $|\varphi| < 76.5°$ for $N = 2f$, $< 75°$ for $N = 4f$, and $< 74.5°$ for $N = 100f$). Natural variability in density stratification can be caused by a complex of varying flows at internal wave, (sub-)mesoscale, seasonal, and decadal scales. This leads to variations in 100-m-scale N of 5-10% and to local variations of up to 20% in small-scale stratification layers: A lot depends on the particular vertical length scale used in the computation of N. It is noted that stratification should last at least a buoyancy- and better an inertial period, to be distinguished from turbulent overturns.

Summing up, overall variations of 10% in β are common for linear semidiurnal internal tides. The associated variation of characteristics slope angle of 0.5°, for mean $N = 10f$, yields a vertical variation O(100) m over a horizontal distance of 10 km. These amounts double when non-traditional effects (2) are considered. A precise localization of persistent "critical" slopes is therefore not possible.

From a geological perspective one may question how, and in what stable equilibrium the shape of topography exists, as internal waves depend on frequency and latitude, but foremost on underwater vertical density stratification. In addition, (linear) internal tides can deform

after interaction with other internal waves such as those generated at over-tidal(-harmonic), near-inertial and near-buoyancy frequencies.

1.3 Sedimentary topography-slope perspective

According to Cacchione et al. (2002), in follow-up from Cacchione and Southard (1974), internal tides are the prime candidate for shaping the ocean's underwater topography, notably its average slope that has approximately the same value as the slope of internal tide characteristics. This is reasoned from the observation that, beyond continental shelves, the average seafloor-slope closely (critically) matches internal tidal characteristics slopes for mean $N \approx 2\times10^{-3}$ s^{-1} around mid-latitudes. Cacchione et al. (2002), considering the upper 1000 m of the ocean mainly, assume N is constant at greater depths, which ignores the continued gradual decrease with increasing depth. However, as will be demonstrated in Section 3, ocean's volume-weighted mean N is three times smaller than the mean value above.

Cacchione et al. (2002) postulate that sediment erosion, and thus prevention of sediment deposition, occur at slopes where the semidiurnal internal tidal slope critically matches that of topography. The internal-wave model by Cacchione and Wunsch (1974) suggests that for such matching slopes the near-bottom flow is strongest. However, their 1D model is based on low vertical mode linear internal waves, adopting only bed shear-stress as means for (inhibition of) resuspension of sediment. Thereby, the effect of plunging breaking waves is not considered (For the effects on sedimentation resuspension due to better known surface wave breaking, see: Voulgaris and Collins, 2000), besides neglects of spring-neap variability, stratification variability and 3D-effects of topography.

As for seafloor topography, the advancement of observational techniques including multibeam acoustic echosounder and satellite altimetry have considerably improved mapping (e.g., Smith and Sandwell, 1997). Using such maps, a global ocean seafloor indexation has been compiled to an overall resolution of 1′ (1852 m in latitude) by Costello et al. (2010). An interesting finding of theirs concerns the separation of ocean area and volume per depth zone.

389 (A correction to area and volume calculations is published in Costello et al. (2015), including
390 a proper definition of depth zone). Whilst 11% of the ocean area and <1% of its volume is
391 occupied by water depths <1000 m, the remarkable results are for the deep sea. It is found that
392 75% of the area and 90% of its volume are in the depth zone with water depths between 3000
393 < H < 6000 m. A large part of this depth zone can be found in the abyssal hill's areas of the
394 Pacific and Atlantic oceans. Only 4.4% of the ocean area and 1.9% of its volume are occupied
395 by the depth zone with water depths between 1000 < H < 2000 m. So, too little topography is
396 in the depth zone of mean N to maintain ocean stratification following the reasoning around
397 ε_{ho}. Expanding to a depth zone of 100 < H < 2000 m, the values are 10% and 2.3%,
398 respectively. We recall that it is the sloping seafloor where most internal waves break and
399 generate turbulence, not the ocean-interior.

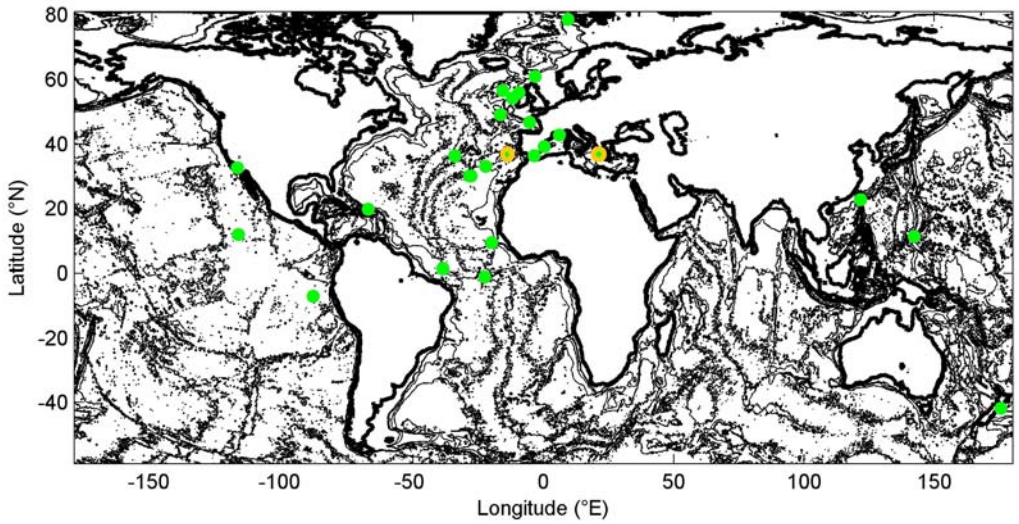

400

401 **Fig. 1**. Global map of seafloor topography (1′-version of Smith and Sandwell, 1997) with
402 contours every 1500 m together with sites (green dots) of NIOZ T-sensor moorings for
403 deep-sea turbulence and internal wave research of which contributions to mean values are
404 used. The two orange encircled sites are discussed in some detail.

405

406 **2 Materials and methods**

407 The foundation of topography-internal wave interaction leading to our ocean turbulence
408 investigation has been an almost three decades-long observational program of a traveling
409 mooring including instrument development and manufacturing. At some 25 sites (Fig. 1)

410 distributed over the global ocean of varying topographic slopes one or more vertical mooring
411 lines were deployed holding custom-made high-resolution low-noise temperature (T-)sensors
412 (van Haren, 2018). The sites showed a large variety in seafloor topography, from abyssal
413 plains to steep canyons, deep trenches, fracture zones, narrow ridges, large continental slopes,
414 and seamounts. Here, sites shallower than continental shelves are not considered, and specific
415 topics like internal wave interaction with sediment waves are not treated (for an example of
416 such see, e.g., van Haren and Puig, 2017).
417
418 *2.1 Moored T-sensors*
419 Some NE-Atlantic sites like Mount Josephine, Rockall Trough and Faeroer-Shetland
420 Channel were occupied with one or more moorings multiple times. The mooring lengths
421 varied between 30 and 1130-m long strings holding a range of 30-760 stand-alone T-sensors
422 at 0.5-2 m intervals, starting between 0.5 and 8 m from the seafloor. The duration of
423 underwater deployment was at least five days, typically several months, and up to three years.
424 The typical mooring was 100-150 m high with 100 T-sensors and was underwater for several
425 months, sampling at a rate of once per second, resulting in the resolution of most energy-
426 containing internal wave and turbulence scales. This allowed for calculation of turbulence
427 values that were averages over most of the relevant scales, in the vertical and over at least
428 inertial and tidal periods include spring-neap cycle. All moorings were held tautly upright
429 after optimizing sufficient buoyancy and low-drag lines, for near-Eulerian measurements. All
430 T-sensors were synchronized every 4 hours to a standard clock, so that vertical profiles were
431 measured almost instantaneously within 0.02 s.
432 The main purpose of the moored T-sensors was to infer turbulence values using the
433 sorting method of Thorpe (1977) over deep-sea topography under varying conditions of
434 elevation, stratification, and local water-flow. The moored instrumentation and data
435 processing are extensively described elsewhere (e.g., van Haren and Gostiaux, 2012; van
436 Haren, 2018). Average turbulence dissipation rate values have been used in Section 1.

Near every mooring, one or more shipborne water column profiles were made using a Conductivity-Temperature-Depth (CTD) package, mainly SeaBird-911. The CTD-data are used to establish the local temperature-density relationship around the depth-range of moored T-sensors, and for reference of absolute temperature and large-scale stratification.

2.2 Seafloor elevation data

Topographic data are retrieved from external data depositories following pioneering works by Smith and Sandwell (1997). Such depositories are GEBCO (https://www.gebco.net) and EMODnet (https://emodnet.ec.europa.eu/en/bathymetry). These data are distributed to grids, e.g., GEBCO-2023 to 15″ (463 m in latitude, North-South direction), and are composites of data from satellite altimetry, shipborne single- and multi-beam acoustic echosounders, and from numerical estimates. Progress is made from the manual soundings of a century ago, via acoustic single-beam echosounder profiling tracks used by Bell (1975a,b), to present-day multibeam mapping and composite global mapping of 1′ (Costello et al., 2010) and smaller. Although the depositories rapidly fill with new high-resolution topographic data following modern multibeam surveys, less than 25% of the seafloor has been mapped at a resolution O(10-100) m so far. The UN-decade initiative SEABED2030 (www.seabed2030.org) aims to complete seabed mapping of the entire ocean before 2030, a challenging goal. It will take at least several decades before the entire seafloor has been mapped at this resolution, if ever. It is noted that the 1′-resolution in some remotely sampled areas results from extrapolated data, while other areas are sampled at 10-100 times higher resolution.

Here, we investigate in some detail topography at two specific sites (Fig. 2) of NE-Atlantic Mount Josephine and E-Mediterranean West-Peloponnese using a variety of 15″-resolution GEBCO data, in conjunction with 3.75″ (116 m in latitude) resolution EMODnet data, and about 1.6″ (50 m in latitude) and 0.375″ (11 m in latitude) resolution multibeam data. The latter are obtained locally around the T-sensor mooring sites only. Our multibeam

data are de-spiked and somewhat smoothed reducing the original sampling rate by a factor of two approximately. The scale variations allow for a limited investigation in slope dependence on horizontal scales.

Although the multibeam echosounder surveys were only a support-part of respective research cruises and therefore do not cover large areas, their extent is sufficient to resolve all internal wave scales. As a bonus, multibeam data processing also delivers information on the reflective properties of the substrate in the property of acoustic backscatter strength. This information was used by van Haren et al. (2015) to demonstrate that over Mount Josephine hard substrates consisting of coarse grain sizes and/or compacted sediment were almost exclusively found in areas with seafloor slopes that were supercritical for semidiurnal internal tides. Less reflective soft substrates consisting of fine grain sizes and/or water-rich sediment were found at sub-critical slopes.

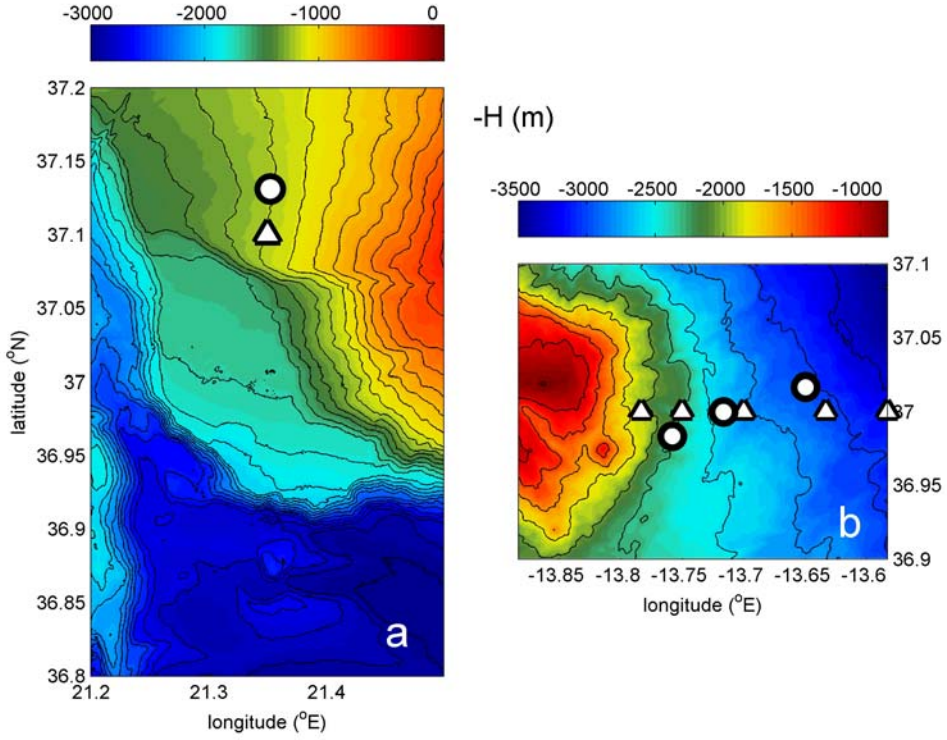

Fig. 2. Two detailed maps made by shipborne multibeam echosounder. (a) Part of West-Peloponnese continental slope, Greece, East-Mediterranean Sea, from R/V Meteor. Circle indicates moored T-sensor location, triangle indicates yoyo-CTD station. Black contours are drawn every 100 m. (b) Part of eastern slope of Mount Josephine, Northeast-Atlantic

Ocean, from R/V Pelagia. Circles indicate moored T-sensor locations, triangles indicate CTD stations during various years. Black contours are drawn every 250 m.

The x-y 2D-gridded, being essentially 3D with z included, seafloor elevation data from above sources will be investigated spectrally, to compare with the 1D single-track, essentially 2D with z included, data from NE-Pacific hills explored by Bell (1975a,b). Some slope statistics is also pursued after computation of the proper slope at each 2D-gridded data-point to characterize the ratio (percentage) of slopes exceeding a particular value. From the total number n_{tot} of 2D-gridded data points per area, we calculate for a particular seafloor slope angle value γ_n the percentage n/n_{tot} of number n of slopes for which $\gamma > \gamma_n$. Its distribution will be compared with that of internal wave, i.c. semidiurnal internal tide, wave characteristics (1), (2) as a function of N, plotted against the ratio of N over the maximum value N_{max} of N.

2.3 Analysis methods

Excursion length,

$$L_e = UT/\pi, \quad (7)$$

is induced by oscillatory particle velocities $U\sin(2\pi t/T)$ over time t, where U, T represent flow speed and -period, respectively. As near-inertial wave period T_f varies with latitude, the two specific sites demonstrate,

$$T_f(|37°|) = 1.8T_{M2}. \quad (8)$$

As a result, for given identical flow speed the inertial excursion length will be 1.8 times larger than that of semidiurnal internal tide. Nonlinear waves may have different lengths. Excursion lengths will be compared with topography elevation spectra below.

As internal wave propagation depends strongly on N, for given latitude and wave frequency, seafloor slopes occurrence statistics should be compared with the ocean's volume-weighted stratification, instead of using vertically averaged N. For ocean volume V(z) per depth zone $[z+0.5\Delta z, z-0.5\Delta z]$ roughly every $\Delta z = 1000$ m as defined in Costello et al. (2010; 2015), a volume weighted buoyancy frequency N_v is calculated as,

509 $N_v(z) = N(z)V(z)/\langle V\rangle$, (9)

510 where <…> denotes averaging over the entire vertical water column.

511

512 **3 Results**

513 The two small deep-sea areas for in-depth investigation are around the same mid-latitudes
514 but otherwise distinctly different (Fig. 2). The NE-Atlantic is known for dominant
515 semidiurnal internal tides besides an-order-of-magnitude smaller amplitude near-inertial
516 waves (van Haren et al., 2016). The East-Mediterranean lacks substantial tides so that internal
517 waves are dominated at near-inertial frequencies only. In the NE-Atlantic, sampling sites are
518 above the eastern side of large underwater Mount Josephine, about 400 km West of Southern
519 Portugal. In the East-Mediterranean, the site is about 20 km West of Peloponnese, Greece.

520

521 *3.1 Vertical profiles*

522 The shipborne water column CTD observations demonstrate moderately stratified and
523 seldom homogeneous waters in the lower 300 m above the seafloor when $N = N_{10}$ is
524 computed over small-scale 10-m vertical scales (Fig. 3a). To get some idea of variability of
525 layering in the ocean, $N = N_{100}$ 100-m scale profiles are given for the NE-Atlantic area in Fig.
526 3b, for comparison. Such variability in length-scale dependent layering is similar in the lower
527 400 m above seafloor in the two areas.

528 In the lower 250 m above seafloor of the East-Mediterranean site, the variability in N-
529 profiles becomes larger than in the interior above, with average values slowly decreasing with
530 depth (Fig. 3a). In the lower 100 m above the seafloor the variability in stratification is
531 largest, both in the vertical and in time. The lower 400 m above the seafloor demonstrate
532 averaged values of $\langle N_{10}\rangle = 7\pm6\times10^{-4}$ s^{-1}, with a gradual decrease of values from 8 to 6×10^{-4} s^{-1}
533 towards the seafloor.

534 Similar mean N-values are observed above Mount Josephine at three times greater depth.
535 At H = 3900 m, $\langle N_{100}\rangle = 7\pm2\times10^{-4}$ s^{-1} is observed in the lower 400 m above the seafloor (Fig.
536 3b). The observed variations in N are about twice larger than sketched in Section 1.2. At a

given pressure level however, the NE-Atlantic site is about half-one order of magnitude more stratified, 2-3 times larger in buoyancy frequency, compared to the East-Mediterranean, and may thus support more internal wave-energy and -shear.

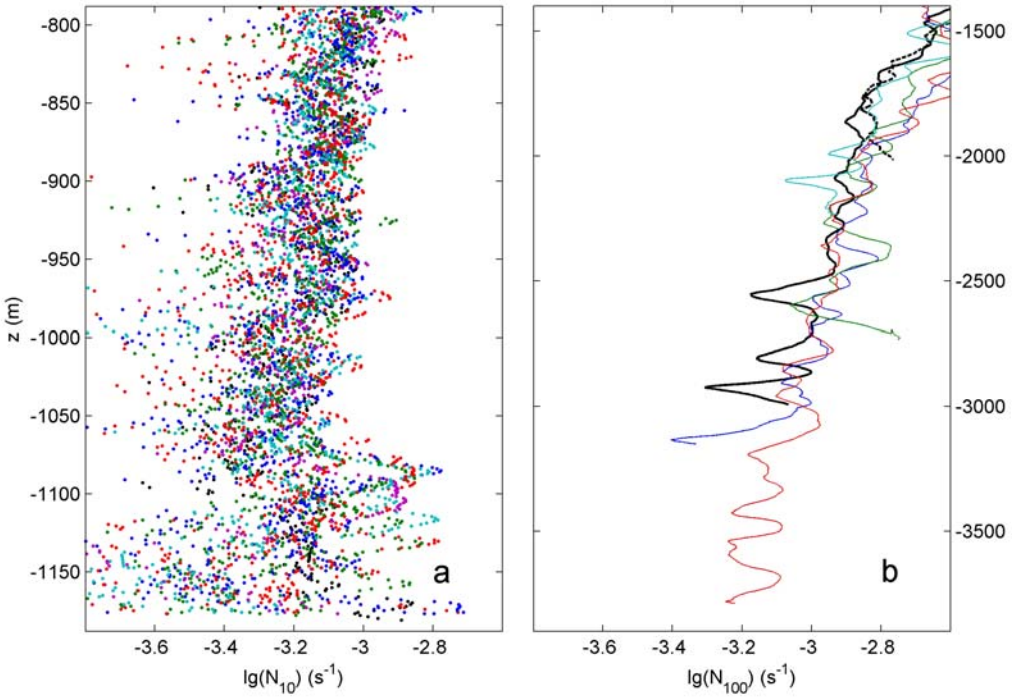

Fig. 3. Logarithm of buoyancy frequency from shipborne water column CTD. (a) One inertial period of 400-m high yoyo-CTD hourly profiles, 19 in total. Computations are made over 10-m vertical scales from fixed location at H = 1180 m water depth in the East-Mediterranean. For clarity, the short-scale profiles are given by coloured dots. (b) Vertical range of 2500 m of profiles from area in van Haren et al. (2015). Computations are made over 100-m vertical scales down to 10 m from various seafloor depths of the eastern slope of Mount Josephine, NE-Atlantic. X-axis scale is identical, but Y-axis scale is different compared to a.

At the deepest NE-Atlantic site considered here, albeit having the mean ocean water depth, the bottom slope is generally subcritical for internal tides (van Haren et al., 2015). This results from the gradual decrease of stratification with depth that leads to a steepening of internal wave characteristics following (1), (2) while the seafloor slope generally becomes

554 smaller for concave topography. To become (super)critical for semidiurnal internal tides, the
555 local slope would need to be (larger than) about 10°.

556 The (semidiurnal tidal) supercritical portion found above Mount Josephine between 1000
557 < H < 2300 m (van Haren et al., 2015) may be part of the 5% of surface-area required to
558 maintain the ocean stratification following ε_H. However, it is not sufficient alone, as this
559 required 5% is larger than, albeit within one standard deviation from, the global total of 4%-
560 surface area of depth zone 1000 < H < 2000 m (Costello et al., 2010; 2015). Because also not
561 all slopes between 1000 and 2000 m are expected to be supercritical (for semidiurnal internal
562 tides even under $N > 2\times10^{-3}$ s^{-1}; Recall that basically all slopes are supercritical for
563 particularly directed near-inertial waves), other supercritical slopes are sought. Supercritical
564 slopes are more easily found at 100-2300 m relatively shallow depths, given the statistically
565 larger N and thus smaller (1), (2), and sufficient turbulence by internal wave breaking.

566 How and where shape internal waves the seafloor? Either the seafloor-shape is concave
567 formed by erosion mid-slope, which, given the general mean stratification profile, leads to
568 less likelihood of turbulent mixing due to internal wave breaking in the deep, or it is convex
569 by erosion above and below, which may favour deeper, supercritical slopes and associated
570 enhanced stretches of mixing. Following nonlinear internal wave 2D-modelling, no distinct
571 difference in turbulence intensity is found between internal wave breaking at convex,
572 concave, or planar slopes (Legg and Adcroft, 2003). However, their model results show
573 relatively large values of energy dissipation at sub-critical slopes, which are not found in
574 ocean observations (e.g., van Haren et al., 2015). It is noted that the above modeling is based
575 on 2D spatial-shapes and ocean topography is essentially 3D, like internal wave propagation
576 and turbulence development. It is thus more generalizing to use full 3D seafloor elevation, i.e.
577 full 2D-slope statistics, and evaluate internal wave breaking with that. While near continental
578 margins, where the continental shelf dives into the continental slope around H = 200 m, the
579 seafloor generally has a convex shape, it generally becomes concave at greater depths. Such

topography would favour relatively shallow supercritical slopes (for semidiurnal internal waves).

3.2 Seafloor spectra

The multibeam echosounder data (Fig. 2) allow for local seafloor investigations, in particular on scale-size and -slopes, that go beyond those of Bell (1975a,b) who used single-beam echosounder data resolving height elevations at horizontal scales O(100) m, with a cutoff at Nyquist wavenumber of about k_{Nyq} = 2.5 cpkm. Bell (1975a,b) established a general seafloor-elevation spectral fall-off rate of k^n, $-2 < n < -5/2$, for $k_0 < k < k_{Nyq}$, with a smaller slope $-1 < n < 0$ for $k = k_0 < 0.1$ cpkm and flattening $n = 0$ for $k < 0.01$ cpkm.

Our multibeam, EMODnet and GEBCO data-sets show a significantly steeper general fall-off rate in elevation spectra (Figs 4a, 5a) than in Bell (1975a,b), with dominant low-wavenumber fall-off at a rate of about k^{-3}, and a saturation to noise values for $k > 10$ cpkm. The steeper spectral fall-off rates may be interpreted as a deviation from random distribution of seafloor elevation, in which energy is no longer uniformly distributed but favoured at the low-wavenumber side and reduced at the high wavenumber side. It has an intermittent appearance (Schuster, 1984).

In detail, the range between $\sim 0.3 < k < \sim 2$ cpkm shows the steepest fall-off rates k^n, $n < -3$, in the East-Mediterranean (Fig. 4), and with extended steep slopes between $\sim 0.55 < k < \sim 6$ cpkm in the NE-Atlantic (Fig. 5). The shift of steep-slope range to higher wavenumbers in the NE-Atlantic area approximately corresponds with the shorter excursion lengths for semidiurnal tides compared to inertial waves following (7), (8), for the same flow speeds. The roll-off to weaker slopes for low wavenumbers is barely resolved, although the spectra do show the same tendency as in Bell (1975a,b). Extended GEBCO_2023-data across the Mid-Atlantic Ridge do resolve and show the roll-off at low wavenumbers (not shown).

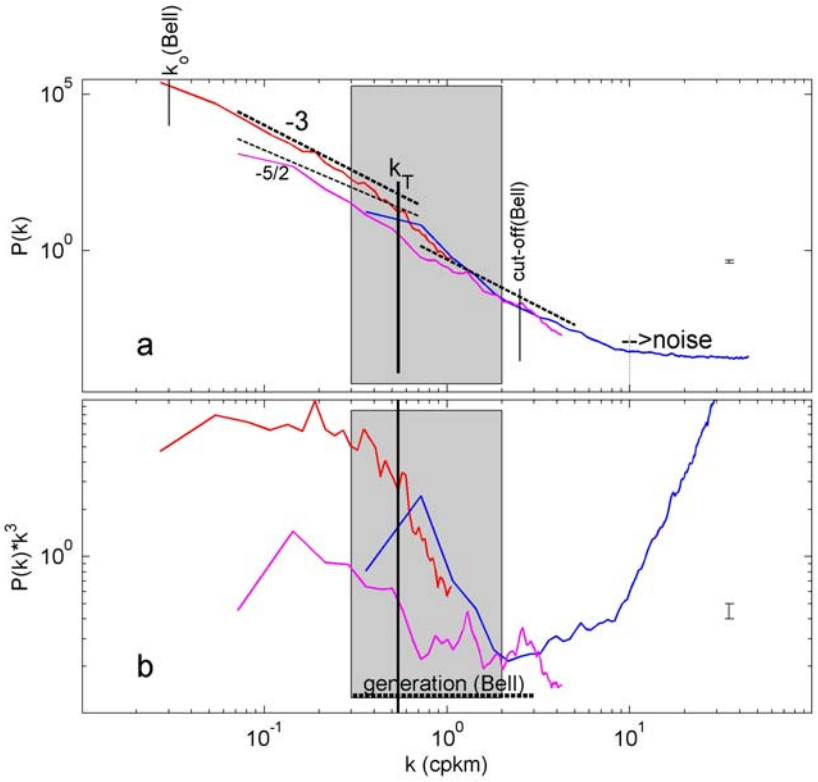

606

607 **Fig. 4**. Spectral analysis of seafloor elevation as a function of horizontal wavenumber k (the
608 inverse of horizontal length-scale L). (a) On the log-log plot matching k^{-3} (-3 on log-log
609 plot) spectral slopes are represented by straight lines, with $k^{-5/2}$ (-5/2-slope) the slope
610 reported by Bell (1975a). Bell's low-wavenumber cut-off k_0 is indicated, albeit barely
611 resolved, as well as high wavenumber roll-off to noise. The central vertical line at transient
612 wavenumber k_T indicates a wavelength of 1852 m (1′ in latitude). The three spectra are for
613 the East-Mediterranean, averages over Fig. 2a: 0.375″ = 11 m sampled multibeam data
614 (blue), 3.75″ = 115 m sampled EMODnet data (magenta), and 15″ = 463 m sampled
615 GEBCO data (red). The grey shading indicates the steep-slope range in which n < -3, for
616 k^n. (b) The same as a., but spectra scaled with k^{-3}, the dominant low wavenumber slope.
617 Bell (1975a,b)'s one-decade range of internal wave generation of Pacific abyssal hills is
618 indicated.

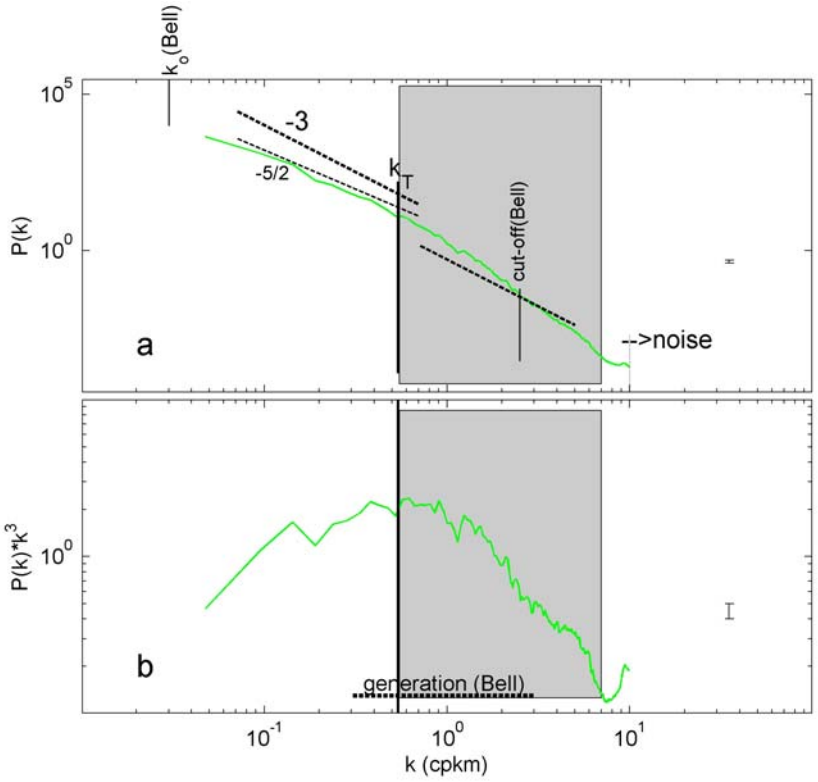

619

620 **Fig. 5**. As Fig.4, but for 1.6″ = 49 m sampled Mount Josephine (NE-Atlantic) multibeam data,
621 average over Fig. 2b. All straight lines are the same as in Fig. 4, but the shaded area is not.
622

623 The steepest fall-off rate is best visible after scaling the spectra, with k^{-3} in Figs 4b, 5b, to
624 better indicate this slump-down in seafloor elevation. Noting that this slump-down does not
625 indicate a spectral gap, the range of strong (steeper) deviation before resuming n = -2.5 or -3
626 centers around transition wavenumber $k_T \approx 0.5$ cpkm, i.e. a wavelength of $L_T \approx 2$ km. It lies in
627 the range of elevation-variance spread that is visible in the data of Bell (1975a,b), and which
628 overlaps with the range of internal wave generation in the abyssal NE-Pacific.

629 Here, it indicates a loss of seafloor topography variance at wavenumber $k > k_T$, by about
630 one order of magnitude (measuring the wavenumber range between the two n = -3 spectral
631 slopes). As the k_T associates with that of the largest internal wave (excursion) scales, one may
632 speculate that the loss of slope elevation relative to general fall-off rate is related with low-
633 frequency internal waves, semidiurnal internal tides, mainly, or near-inertial waves having
634 larger period (8) than M_2-tides at $|\varphi| = 37°$, and their erosive turbulence generation smoothing

635 out topography sizes. The spectral slump-down around k_T is statistically significant. However,
636 it also significantly varies between different sites, shifting about half an order of magnitude to
637 higher wavenumbers at Mount Josephine. This may relate with the dominance of 1.8-times
638 larger excursion length (~inverse wavenumber) of near-inertial waves in the East
639 Mediterranean, for fixed flow speed. Possibly, the excursion length of nonlinear breaking
640 internal waves is different for each site and different with dominant wave frequencies, being
641 inertial or tidal. Excursion length varies perhaps most with local flow speed in other areas.
642 For general GEBCO_2023 data from across the Mid-Atlantic Ridge in comparison with our
643 data, one finds also strict k^{-3} spectral fall-off rate and the spectral slump-down shifts by half
644 an order of magnitude to lower wavenumbers (not shown).
645
646 *3.3 Slope statistics*
647 The mean slope of seafloor topography calculated by Bell(1975a,b) at >100-m scales is
648 3±1°. In our two small areas around the same latitude (Fig. 2), the slope distribution varies
649 with length-scale; at slopes > 3°, the shorter the length-scales the steeper slopes are calculated
650 (Fig. 6). The 3°-slope is the median seafloor-slope value for our small East-Mediterranean
651 site, irrespective of scales used (Fig. 6a). The median seafloor-slope value for our small NE-
652 Atlantic site varies per scale and is about 4° at 1′-resolution and 5° at 0.25′-resolution (Fig.
653 6b). These slopes are found for common mean N at z < -2000 m.
654 For most of the global ocean using a 1′-resolution, Costello et al. (2010) find that 9.4% of
655 the seafloors have a slope between 2 and 4°, 8.2% have a slope > 4° and 4.5% have a slope >
656 6°. From which we conclude that 3.7% have a slope between 4° and 6°. Recall that 75% of
657 the ocean area and 90% of its volume has seafloors between 3000 and 6000 m, where thus
658 most of these slope(percentage)s are.
659

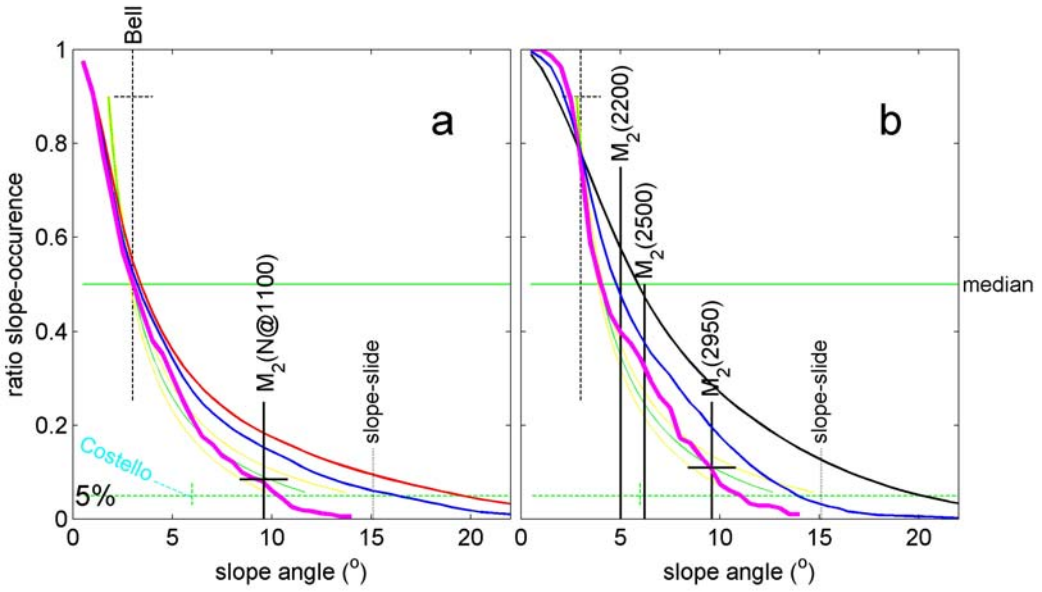

Fig. 6. Seafloor statistics curves of ratio of slope occurrence, percentage of slopes being larger than particular slope angle (Section 2.2), for different seafloor-elevation sampling scales. For comparison, graphs are plotted for M_2 internal tide characteristic slopes as a function of N against normalized N/N_{max}, one in green using (1) and two in yellow using (2). The horizontal center green line indicates the median, the lower horizontal dashed-green line indicates the 0.05(5%) level that is required for (just-)supercritical slopes to generate sufficient global turbulence. Vertical black-dashed lines indicate Bell (1975b)'s average slope of NE-Pacific abyssal hills and the maximum slope before collapse of sediment packing 'slope-slide'. (a) From East-Mediterranean map of Fig. 2a using three different scales for elevation slope-computations: L = 1′ (magenta), 15″ (blue) and 3.75″ (red). Costello et al.'s (2010) range of percentages is indicated in light-blue (see text). The semidiurnal lunar (M_2) internal tide slope is indicated for local N at H = 1100 m, with corresponding error/spread in characteristics value. (b) From NE-Atlantic map of Fig. 2b using L = 1′ (magenta), 14.5″ (blue) and 1.6″ (black). M_2-slopes for three different mooring sites are indicated as a function of their H (m).

At our two sites, slopes are slightly steeper at 1′-resolution, and 5% of the seafloors have slopes > 10°. For the East-Mediterranean, at 1′-resolution the (semidiurnal tidal) critical slope is 9.6° for local $N = 6.6\times10^{-4}$ s^{-1}. This value of N is to within error the same value found for

680 N_v after volume-weighted averaging from (9) below z < -500 m of near-surface seasonal
681 stratification variation for open NE-Atlantic and Mariana Trench (Pacific Ocean) CTD
682 observations (Fig. 7). It is noted that this volume-weighted averaging includes effects of
683 Antarctic Bottom Water, observed in the Mariana Trench profile. The value of N_v is three
684 times smaller than the mean buoyancy frequency used by Cacchione et al. (2002).

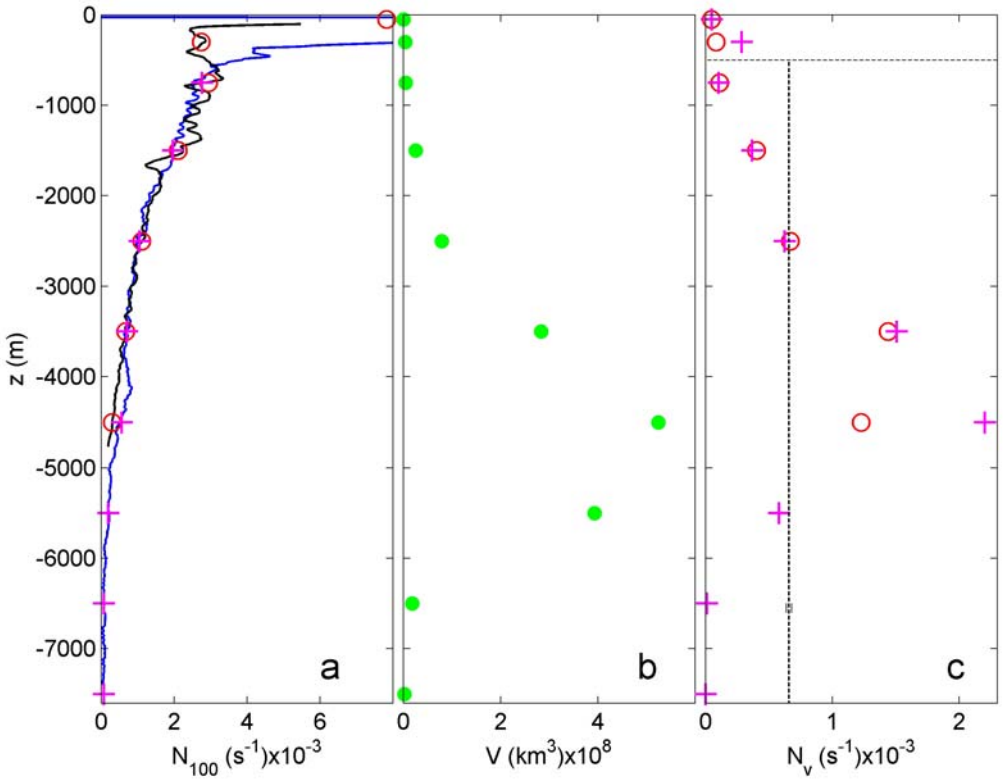

685

686 **Fig. 7**. Weighted function of buoyancy frequency as a function of the vertical. (a) Large-100-
687 m scale buoyancy frequency from NE-Atlantic, off Mount Josephine (green profile with
688 red circles) from the area in van Haren et al. (2015), and over and inside Mariana Trench
689 (blue with magenta plusses) from (van Haren et al., 2017; van Haren et al., 2021). (b)
690 Ocean volume V(z) per depth zone, adapted from Costello et al. (2010) with depth zones
691 defined in Costello et al. (2015). (c) Volume-weighted values of buoyancy frequency in (a)
692 following (9) using V(z) in (b). Note the relatively large value from around -4500 m in
693 Mariana Trench data that is associated with Antarctic Bottom Water. Below z < -500 m,
694 the vertical dashed line indicates mean value $<N_v> = 6.6 \pm 0.2 \times 10^{-4}$ s^{-1}, for both profiles,
695 with small error bar.
696

At this volume-weighted average N_v, associated supercritical slopes for semidiurnal lunar internal tide are found to occur for 5% of all slope values, i.e. 5% of all slopes are > 9.6° (Fig. 6a). This percentage is reached at an angle of 20° for 1.6″-resolution multibeam data of Mount Josephine (Fig. 6b). As this angle-value is steeper than that for sedimentary stability, its seafloor texture may thus foremost consist of hard substrate, which indeed has been observed in multibeam data for supercritical slopes (van Haren et al., 2015).

However, when computed at the larger 1′-resolution (magenta graphs in Fig. 6) one finds a 5%-transition for 11°, which is to within error the same slope for NE-Atlantic and East-Mediterranean multibeam data. Thus, seafloor slope statistics are identical to within error between our two sites at 1′-resolution. Recall that the 1′-resolution is close to the spectral transition length-scale $1/k_T$ (Figs 4, 5), and close to the internal tidal (largest internal wave) excursion length for typical deep-sea flow speed. The characteristics (2) slope-range between 9 and 11° comprises the 10° seafloor-slope above which semidiurnal internal tides become supercritical at sites of the 3900-m mean ocean water depth given local N. Although this N is found around 1100 m in the East-Mediterranean, the approximate 2.5 times weaker N, compared with NE-Atlantic data at the same depth, associate with the lack of tides so that inertial energy is about 40% of total (inertial and tidal) internal wave energy found in the NE-Atlantic.

Although volume-weighted mean N_v and thus mean internal tidal characteristics slopes are found in the depth zone of mean ocean depth comprising 75% of the ocean area (Costello et al., 2010), the occurrence of 5% supercritical slopes diminishes local relatively weak turbulence dissipation rates $O(10^{-9})$ m^2 s^{-3} to a small contribution <10% to maintain global ocean stratification. However, the coincidence of 5% seafloor slopes with supercritical slopes for volume-weighted mean N and N at mean ocean depth may reflect an ocean-wide balance of internal wave-turbulence and topography interaction. Locally in the deep-sea, such turbulence may have considerable influence for redistribution of sediment and nutrients. Examples are short-term contributions of inertial waves generated by, e.g., large storms such

as typhoons. For standard mean 10^{-8} m^2s^{-3} over h = 200 m in H = 3900 m, 5% semidiurnal tidal supercritical slopes yield a global contribution of 2.5×10^{-11} m^2 s^{-3}. A passing typhoon may dissipate 10^{-7} m^2s^{-3} as observed (van Haren et al., 2020) over h = 200 m in H = 3100 m at any slope, as basically all slopes are super-critical for a near-inertial wave characteristic.

Considering the more numerous moored T-sensor observations from the depth zone 100-2000 m, which comprises 10% of the ocean area (Costello et al., 2010; 2015), the larger local N yields 50% of local slopes to be supercritical (for semidiurnal tides), cf. Fig. 6. The overall 50% of 10% = 5% supercritical slopes are sufficient to maintain the entire ocean stratification over typical h = 100 m in average H =1000 m and observed turbulence dissipation rate ε_{ho}. This is also the depth zone in which cold water corals (CWC) thrive (United Nations, 2017). The suspension feeding CWC rely on nutrient supply via sufficiently turbulent hydrodynamic processes.

4 Discussion

Cacchione et al. (2002) made calculations with water-level height mean N above a mean-depth ocean seafloor, holding mean-N value constant for all z < -150 m. This is not representing a realistic internal wave turbulence environment, because (1) N monotonically decreases with depth (except under local conditions such as when Antarctic Bottom waters are found near 4000 m), (2) internal waves refract so that local N has to be accounted for, (3) internal waves predominantly break at sloping seafloor and not in the ocean-interior.

It is well established that internal tidal dissipation mainly occurs over steep topography (e.g., Jayne et al., 2004). However, these authors emphasize that [global modelling efforts] still lack a high resolution bathymetry data set to improve our ability to better quantify ocean mixing, and understand its impact on the Earth's climate. It may well take considerable effort and time until we have mapped the seafloor to the same detail as the surface of Mars (Smith, 2004).

Deep-ocean internal waves can be modelled to first order as linear waves and are found ubiquitous throughout all seas and oceans. However, given their natural environment which is

752 not constant in space and time and their potential interactions with other water-flows they
753 divert considerably from linear, constant-frequency waves. First, the stratification-support
754 varies under internal wave straining, boundary flows and (sub-)mesoscale eddies, so that N
755 shows a relative variation of typically ±20%. Although semidiurnal internal tides are
756 dominant energetically, their variation in frequency alone provides 6% variations in slope of
757 characteristics. In the deep-sea, roughly the deeper half of all oceans, $N < 8f$, at mid-latitudes,
758 and full internal wave equations show a spread in internal tide characteristics of >15%. All
759 these natural variations, not counting variations in seafloor slope determination as a function
760 of length-scale, provide a relative error-range in dominant internal wave characteristics of 25-
761 50%.

762 It thus seems impossible to find a particular persistent critical slope for a given single
763 internal wave frequency on a 1′-scale, and which also ignores the highly nonlinear character
764 of dominant turbulence-generating upslope propagating bores, which are composed of
765 motions at many internal wave frequencies. Therefore, it is not surprising that most internal
766 wave generated turbulence occurs at (just) super-critical slopes, which provides a broader
767 slope- and thus frequency-range.

768 As the above relative uncertainty range of internal wave characteristics matches that of
769 relative error of about 33% (factor of 2) in mean turbulence dissipation rates, it reflects the
770 uncertainty in determining present-day percentage of supercritical slopes required to maintain
771 ocean stratification, being 5±1.5% for seas where internal tides dominate. This uncertainty
772 also sets the bounds for robustness of the internal wave-topography interactions: It is the
773 margin within which variations are expected to find sufficient feed-back not to disrupt the
774 system from some equilibrium.

775 If so, spiking any variations to this system must go beyond an energy variation of about
776 30%, which is larger than (the determination of) tidal variation but probably less than inertial
777 motions variations, say wind (Wunsch and Ferrari, 2004). In terms of stratification, 30% of
778 variation is feasible near the sea-surface via seasonal but also day-night variations, but is well
779 exceeding any natural stratification variations in the deep-sea, say for $z < -500$ m.

Suppose we can go beyond 30% variation, what will happen then? It takes at least decades-centuries-millennia for the seafloor elevation to adapt to an equilibrium of sufficiently supercritical slopes. If N increases by >30% uniformly throughout the ocean, more (higher frequency) internal waves will be supported and internal tide characteristics will become flatter. As a result, more (unaltered) seafloor slopes will become supercritical, which will raise the amount of ocean turbulence. Perhaps by >30%. Increased turbulence means more heat transport, hence a reduction of N that diminishes the initial 30%-increase. It goes without saying that the opposite occurs in the event of a decrease in N.

Although being a meagre proof of evidence, we recall that the (East-)Mediterranean deep-sea has a factor of 2-3 times weaker N than the tidally dominated NE-Atlantic Ocean at any given depth. This factor is commensurate with the 2-3 times weaker near-inertial internal wave energy compared with that of combined energy of internal tide and near-inertial waves. Both sea-areas are in present-day equilibrium. As a result, it seems that it is not the buoyancy (density stratification) variations that strongly disturb the equilibrium, but the external sources of internal wave (kinetic energy).

(Just-)super-critical slopes are probably bounded by a maximum of 15° for sedimentary slope-instability. At any rate, the super-critical seafloor slopes allow development of upslope propagating bores and rapid restratification of the back-and-forth sloshing internal tides. In contrast with foreward wave-breaking at a beach, internal tides break backwards at a slope (van Haren and Gostiaux, 2012). This may explain a lack of clear swash, i.e., while upslope propagating bores may be considered as uprush, a clear vigorous backwash is not observed during the downslope warming tidal phase near the seafloor in moored T-sensor data. This demonstrates a discrepancy with the 2-D modelling of Winters (2015). While in the model most intense turbulence is found near the seafloor during the downslope phase expelling into the interior, ocean observations demonstrate largest turbulence around the upslope propagating backwards breaking bore, with the bore sweeping material up from the seafloor (Hosegood et al., 2004). Probably some 3D- or rotational aspect is important for ocean internal wave breaking, yet to be modelled.

We have considered a combination of seafloor elevation and internal wave turbulence data to revisit the interaction between topography and water flows in the deep-sea. From various perspectives including turbulence values, vertical density stratification, (water) depth zones, and seafloor and internal wave slopes and scale-lengths it is found that interaction is relatively stable, whereby mainly internal tides and near-inertial waves shape the topography to within 30% variability.

5 Conclusions

The median value of seafloor slope of 3±0.2° from multibeam echosounder and satellite data from NE-Atlantic, mid-Atlantic Ridge and East-Mediterranean sites closely matches the half-a-century-ago established rms-mean slope of 3±1° from single-beam echosounder data across NE-Pacific abyssal hills (Bell, 1975a,b). Our result is found only weakly dependent of scale, which we varied between 0.027′ and 1′. It lends some robustness to the determination of seafloor slopes, for horizontal scales that match dominant internal wave excursion lengths.

The average spectral fall-off rate of seafloor elevation is found steeper than Bell's (1975a,b), which indicates a non-uniform distribution of scales instead of a uniform distribution as previously suggested. In particular, the spectral slump-down around a length-scale of 2 km is noted, which suggests a lack of seafloor elevation shaped by the largest internal wave excursion length dissipating its energy into turbulence creating sediment erosion. This spectral slump-down is found in seafloor elevation data from both the NE-Atlantic, where semidiurnal internal tides prevail, and, at somewhat smaller values, from the East-Mediterranean, where tides are small and near-inertial motions that have 1.8 times larger length scales dominate internal waves. In the East-Mediterranean, the buoyancy frequency is found smaller than at corresponding depths in the NE-Atlantic, which is commensurate with the contribution of internal tides (and lack thereof).

Recent moored high-resolution T-sensor data demonstrated that internal wave breaking is found most vigorously above seafloor slopes that are supercritical rather than much more

limiting critical for (semidiurnal) internal tides, with local turbulence dissipation rate > 10^{-7} m^2s^{-3} in depth zone 100 < H < 2200 m (NE-Atlantic). This depth zone hosts most of cold-water corals that depend on vigorous turbulence for nutrient supply. Our seafloor statistics show that 50% of the slopes are supercritical for stratification in this depth zone, which compensates for the depth zone's occupation of only 10% of ocean area. As a result, we find that internal wave breaking at 5±1.5% of slopes suffices to maintain global ocean density stratification.

In greater depth zones, internal wave breaking is generally less turbulent contributing <10% to maintain global stratification mainly due to steeper internal tidal characteristics slopes. Even in the deep-sea however, 5% of seafloor slopes coincide with supercritical slopes for volume-weighted mean N_v, and N at mean ocean depth, supporting an ocean-wide balance of topography and internal wave-turbulence interaction. Turbulence may be locally important for the redistribution of heat, nutrients, and oxygen, e.g., during the passage of typhoons generating near-inertial waves as most seafloor slopes are supercritical for (one characteristic of) such waves, also in great depth zones.

Data availability. Seafloor elevation data are extracted from depositories https://www.gebco.net and https://emodnet.ec.europa.eu/en/bathymetry. Raw East-Mediterranean CTD data supporting the results of this study are available in database https://data.mendeley.com/datasets/6td5dxf6bj/1.

Author contribution: HvH designed the experiments, while HvH and HdH carried them out. HvH focused on the oceanographic part, HdH on the topographic and sedimentology part. HdH verified that figures are colour-blind friendly HvH prepared the manuscript with contributions from HdH.

Competing interests. The authors have no conflicts to disclose.

862

863 *Ackowledgments.* NIOZ T-sensors were supported in part by NWO, the Netherlands
864 Organization for the advancement of science. We thank NIOZ-MRF and the captains and
865 crews of the R/V's Pelagia and Meteor, as well as from numerous other research vessels we
866 joined, for their very helpful assistance during mooring construction and deployment.

867

868 **References**

869 Alford, M. H.: Improved global maps and 54-year history of wind-work on ocean inertial
870 motions, Geophys. Res. Lett., 30, 1424, 2003.

871 Armi, L.: Effects of variations in eddy diffusivity on property distributions in the oceans, J.
872 Mar. Res., 37, 515-530, 1979.

873 Bell, T. H. Jr.: Topographically generated internal waves in the open ocean, J. Geophys. Res.,
874 80, 320-327, 1975a.

875 Bell, T. H. Jr.: Statistical features of sea-floor topography, Deep-Sea Res., 22, 883-892,
876 1975b.

877 Cacchione D. A., and Southard, J. B.: Incipient sediment movement by shoaling internal
878 gravity waves, J. Geophys. Res., 79, 2237-2242, 1974.

879 Cacchione, D. A., and Wunsch, C.: Experimental study of internal waves over a slope, J.
880 Fluid Mech., 66, 223-239, 1974.

881 Cacchione, D. A., Pratson, L. F., and Ogston, A. S.: The shaping of continental slopes by
882 internal tides, Science, 296, 724-727, 2002.

883 Chen, H., Zhang, W., Xie, X., Gao, T., Liu, S., Ren, J., Wang, D., and Su, M.: Linking
884 oceanographic processes to contourite features: Numerical modelling of currents
885 influencing a contourite depositional system on the northern South China Sea margin,
886 Mar. Geol., 444, 106714, 2022.

887 Costello, M. J., Cheung, A., and de Hauwere, N.: Surface area and the seabed area, volume,
888 depth, slope, and topographic variation for the world's seas, oceans, and countries,
889 Environ. Sci. Technol., 44, 8821-8828, 2010.

890 Costello, M. J., Smith, M., and Fraczek, W.: Correction to Surface area and the seabed area,
891 volume, depth, slope, and topographic variation for the world's seas, oceans, and
892 countries, Environ. Sci. Technol., 49, 7071-7072, 2015.

893 Dillon, T. M.: Vertical overturns: a comparison of Thorpe and Ozmidov length scales, J.
894 Geophys. Res., 87, 9601-9613, 1982.

Dushaw, B. D.: Mapping low-mode internal tides near Hawaii using TOPEX/POSEIDON altimeter data, Geophys. Res. Lett., 29, 1250, 2002.

Eriksen, C. C.: Observations of internal wave reflection off sloping bottoms, J. Geophys. Res., 87, 525-538, 1982.

Eriksen, C. C.: Implications of ocean bottom reflection for internal wave spectra and mixing. J. Phys. Oceanogr., 15, 1145-1156, 1985.

Ferrari, R., Mashayek, A., McDougall, T. J., Nikurashin, M., and Campin, J.-M.: Turning ocean mixing upside down, J. Phys. Oceanogr., 46, 2229-2261, 2016.

Garrett, C.: The role of secondary circulation in boundary mixing, J. Geophys. Res., 95, 3181-3188, doi:10.1029/JC095iC03p03181, 1990.

Gerkema, T., Zimmerman, J. T. F., Maas, L. R. M., and van Haren, H.: Geophysical and astrophysical fluid dynamics beyond the traditional approximation, Rev. Geophys., 46, RG2004, doi:10.1029/2006RG000220, 2008.

Gregg, M. C.: Scaling turbulent dissipation in the thermocline, J. Geophys. Res., 94, 9686-9698, 1989.

Hosegood, P., Bonnin, J., and van Haren, H.: Solibore-induced sediment resuspension in the Faeroe-Shetland Channel, Geophys. Res. Lett., 31, L09301, doi:10.1029/2004GL019544, 2004.

Jayne, S. R., St. Laurent, L. C., and Gille, S. T.: Connections between ocean bottom topography and Earth's climate, Oceanography, 17(1), 65-74, 2004.

King, B., Stone, M., Zhang, H. P., Gerkema, T., Marder, M., Scott, R. B., and Swinney, H. L.: Buoyancy frequency profiles and internal semidiurnal tide turning depths in the oceans, J. Geophys. Res., 11, C04008, doi:10.1029/2011JC007681, 2012.

Klymak J. M., and Moum, J. N.: Internal solitary waves of elevation advancing on a shoaling shelf, Geophys. Res. Lett., 30, 2045, doi:10.1029/2003GL017706, 2003.

Kunze, E.: Near-inertial wave propagation in geostrophic shear, J. Phys. Oceanogr., 15, 544-565, 1985.

922 Kunze, E.: Internal-wave-driven-mixing: Global geography and budgets, J. Phys. Oceanogr.,
923 47, 1325-1345, 2017.
924 LeBlond, P., and Mysak, L. A.: Waves in the Ocean, Elsevier, Amsterdam, 602 pp, 1978.
925 Legg, S., and Adcroft, A.: Internal wave breaking at concave and convex continental slopes,
926 J. Phys. Oceanogr., 33, 2224-2246, 2003.
927 Munk, W. H.: Abyssal recipes, Deep-Sea Res., 13, 707-730, 1966.
928 Munk W., and Wunsch, C.: Abyssal recipes II: Energetics of tidal and wind mixing, Deep-Sea
929 Res. I, 45, 1977-2010, 1998.
930 Oakey, N. S.: Determination of the rate of dissipation of turbulent energy from simultaneous
931 temperature and velocity shear microstructure measurements, J. Phys. Oceanogr., 12,
932 256-271, 1982.
933 Osborn, T. R.: Estimates of the local rate of vertical diffusion from dissipation measurements,
934 J. Phys. Oceanogr., 10, 83-89, 1980.
935 Polzin, K. L., Toole, J. M., Ledwell, J. R., and Schmitt, R. W.: Spatial variability of turbulent
936 mixing in the abyssal ocean, Science, 276, 93-96, 1997.
937 Puig, P., Ogston, A. S., Guillén, J., Fain, A. M. V., and Palanques, A.: Sediment transport
938 processes from the topset to the foreset of a crenulated clinoform (Adriatic Sea), Cont.
939 Shelf Res., 27, 452-474, 2007.
940 Ray, R. D., and Zaron, E. D.: M_2 internal tides and their observed wavenumber spectra from
941 satellite altimetry, J. Phys. Oceanogr., 46, 3-22, 2016.
942 Rebesco, M., Hernández-Molina, F. J., van Rooij, D., and Wåhlin, A.: Contourites and
943 associated sediments controlled by deep-water circulation processes: State-of-the-art and
944 future considerations, Mar. Geol., 352, 111-154, 2014.
945 Sarkar, S., and Scotti, A.: From topographic internal gravity waves to turbulence, Ann. Rev.
946 Fluid Mech., 49, 195-220, 2017.
947 Schuster, H. G.: Deterministic Chaos: An Introduction, Physik Velag, Weinheim, Germany,
948 220 pp, 1984.

949 Smith, W. H. F.: Introduction to this special issue on bathymetry from space, Oceanography,
950 17(1), 6-7, 2004.
951 Smith, W. H. F., and Sandwell, D. T.: Global seafloor topography from satellite altimetry and
952 ship depth soundings, Science, 277, 1957-1962, 1997.
953 St. Laurent, L., Alford, M. H., and Paluszkiewicz, T.: An introduction to the special issue on
954 internal waves, Oceanography 25(2), 15-19, 2012.
955 Thorpe S. A.: Turbulence and mixing in a Scottish Loch, Phil. Trans. Roy. Soc. A, 286, 125-
956 181, 1977.
957 Thorpe, S. A.: Transitional phenomena and the development of turbulence in stratified fluids:
958 a review, J. Geophys. Res., 92, 5231-5248, 1987.
959 Trincardi, F., and Normark, W. R.: Sediment waves on the Tiber pro-delta slope, Geo-Mar.
960 Lett., 8, 149-157, 1988.
961 United Nations, ed.: Cold-Water Corals, In: The First Global Integrated Marine Assessment:
962 World Ocean Assessment I. Cambridge University Press, 803-816, 2017.
963 van Haren, H.: Philosophy and application of high-resolution temperature sensors for
964 stratified waters, Sensors, 18, 3184. doi:10.3390/s18103184, 2018.
965 van Haren, H.: Open-ocean interior moored sensor turbulence estimates, below a Meddy,
966 Deep-Sea Res. I, 144, 75-84, 2019.
967 van Haren, H., and Gostiaux, L.: Energy release through internal wave breaking,
968 Oceanography 25(2), 124-131, 2012.
969 van Haren, H., and Puig, P.: Internal wave turbulence in the Llobregat prodelta (NW
970 Mediterranean) under stratified conditions: A mechanism for sediment waves generation?
971 Mar. Geol., 388, 1-11, 2017.
972 van Haren, H., Maas, L., Zimmerman, J. T. F., Ridderinkhof, H., and Malschaert, H.: Strong
973 inertial currents and marginal internal wave stability in the central North Sea, Geophys.
974 Res. Lett., 26, 2993-2996, 1999.
975 van Haren, H., Cimatoribus, A. A., and Gostiaux, L.: Where large deep-ocean waves break,
976 Geophys. Res. Lett., 42, 2351-2357, doi:10.1002/2015GL063329, 2015.

977 van Haren, H., Cimatoribus, A. A., Cyr, F., and Gostiaux, L.: Insights from a 3-D temperature
978 sensors mooring on stratified ocean turbulence, Geophys. Res. Lett., 43, 4483-4489,
979 doi:10.1002/2016GL068032, 2016.
980 van Haren, H., Berndt, C., Klaucke, I.: Ocean mixing in deep-sea trenches: new insights from
981 the Challenger Deep, Mariana Trench, Deep-Sea Res. I, 129, 1-9, 2017.
982 van Haren, H., Chi, W.-C., Yang, C.-F., Yang, Y. J., and Jan, S.: Deep sea floor observations
983 of typhoon driven enhanced ocean turbulence, Progr. Oceanogr., 184, 102315, 2020.
984 van Haren, H., Uchida, H., Yanagimoto, D.: Further correcting pressure effects on SBE911
985 CTD-conductivity data from hadal depths, J. Oceanogr., 77, 137-144, 2021.
986 van Haren, H., Mienis, F., and Duineveld, G.: Contrasting internal tide turbulence in a
987 tributary of the Whittard Canyon, Cont. Shelf Res. 236, 104679, 2022.
988 Voulgaris, G., and Collins, M. B.: Sediment resuspension on beaches: response to breaking
989 waves, Mar. Geol., 167, 167-187, 2000.
990 Watanabe, M., and Hibiya, T.: Global estimates of the wind-induced energy flux to inertial
991 motions in the surface mixed layer, Geophys. Res. Lett., 29, 1239,
992 doi:10.1029/2001GL014422, 2002.
993 Winters, K. B.: Tidally driven mixing and dissipation in the stratified boundary layer above
994 steep submarine topography, Geophys. Res. Lett., 42, 7123-7130, 2015.
995 Wüst, G.: The Stratosphere of the Atlantic Ocean. Scientific Results of the German Atlantic
996 Expedition of the Research Vessel Meteor, 1925-27, Vol. VI, Section 1, English
997 translation, W. J. Emery (ed.). Amerind Pub. Co., New Delhi, 1978, 1935.
998 Wunsch, C.: On oceanic boundary mixing, Deep-Sea Res., 17, 293-301, 1970.
999 Wunsch, C., and Ferrari, R.: Vertical mixing, energy, and the general circulation of the
1000 oceans, Annu. Rev. Fluid Mech., 36, 281-314, 2004.
1001 Wunsch, C.: Modern observational physical oceanography: Understanding the global ocean,
1002 Princeton University Press. 512 pp, 2015.
1003